Article:
Wang, N., Rumney, R.M.H., Yang, L. et al. (4 more authors) (2013) The P2Y13 receptor regulates extracellular ATP metabolism and the osteogenic response to mechanical loading. Journal of Bone and Mineral Research, 28 (6). pp. 1446-1456. ISSN 0884-0431

https://doi.org/10.1002/jbmr.1877

Title: The P2Y13 receptor regulates extracellular ATP metabolism and the osteogenic response to mechanical loading.

Ning Wang, Ph.D[a], Robin M.H. Rumney, Ph.D[a], Lang Yang[a], Bernard Robaye, Ph.D[b], Jean-Marie Boeynaems, Ph.D[b,c], Timothy M. Skerry, Ph.D[a], Alison Gartland, Ph.D[a1]

[a]The Mellanby Centre for Bone Research**,** Department of Human Metabolism, The University of Sheffield, Sheffield, UK, [b]Institute of Interdisciplinary Research, IRIBHM, Université Libre de Bruxelles, Gosselies, Belgium, [c]Department of Laboratory Medicine, Erasme Hospital, Brussels, Belgium

Funding Source: European Commission under the 7th Framework Programme (proposal #202231) performed as a collaborative project among the members of the ATPBone Consortium (Copenhagen University, University College London, University of Maastricht, University of Ferrara, University of Liverpool, University of Sheffield, and Université Libre de Bruxelles), and is a sub study under the main study "Fighting osteoporosis by blocking nucleotides: purinergic signalling in bone formation and homeostasis"

1 Corresponding author and address for reprint requests:
Dr Alison Gartland,
The Mellanby Centre for Bone Research
Department of Human Metabolism
The University of Sheffield
Beech Hill Road
Sheffield, S10 2RX
UK
Phone: (+44) 0114 226 1435
Fax: (+44) 0114 271 1711
Email: a.gartland@sheffield.ac.uk

No supplemental data has been included with the submission

Disclosure Page

All authors state that they have no conflicts of interest.

Abstract

ATP release and subsequent activation of purinergic receptors has been suggested to be one of the key transduction pathways activated by mechanical stimulation of bone. The $P2Y_{13}$ receptor, recently found to be expressed by osteoblasts, has been suggested to provide a negative feedback pathway for ATP release in different cell types. Therefore, we hypothesised that the $P2Y_{13}$ receptor may contribute to the mediation of osteogenic responses to mechanical stimulation by regulating ATP metabolism by osteoblasts. To test this hypothesis, wild type (WT) and $P2Y_{13}$ receptor knock-out ($P2Y_{13}R^{-/-}$) mice were subject to non-invasive axial mechanical loading of the left tibiae to induce an osteogenic response. Micro-Computed Tomography analysis showed mechanical loading induced an osteogenic response in both strains of mice in terms of increased total bone volume and cortical bone volume, with the $P2Y_{13}R^{-/-}$ mice having a significantly greater response. The extent of the increased osteogenic response was defined by dynamic histomorphometry data showing dramatically increased bone formation and mineral apposition rates in $P2Y_{13}R^{-/-}$ mice compared with controls. In vitro, primary $P2Y_{13}R^{-/-}$ osteoblasts had an accumulation of mechanically induced extracellular ATP and reduced levels of hydrolysis. In addition, $P2Y_{13}R^{-/-}$ osteoblasts also had a reduction in their maximal alkaline phosphatase (ALP) activity, one of the main ecto-enzymes expressed by osteoblasts which hydrolyses extracellular ATP. In conclusion, deletion of the $P2Y_{13}$ receptor leads to an enhanced osteogenic response to mechanical loading in vivo, possibly due to the reduced extracellular ATP degradation by ALP. The augmented osteogenic response to mechanical stimulation, combined with suppressed bone remodelling activities and protection from OVX-induced bone loss after $P2Y_{13}$ receptor depletion as previously described, suggests a potential role for $P2Y_{13}$ receptor antagonist-based therapy, possibly in combination with mechanical loading, for the treatment of osteoporosis.

Key words: P2Y13 receptor, osteogenic, mechanical loading, ATP release, ATP hydrolysis

Introduction

Bone integrity is maintained throughout life via bone remodelling where the balance between bone resorption and formation is critical. Altered coupling of resorption and formation leads to bone disorders such as osteoporosis which is characterized by higher resorption and lower formation (1). Most current treatment strategies for osteoporosis have focused on anti-resorptive therapies such as bisphosphonates and more recently antibodies to RANKL (Denosumab) which can successfully reduce the risk of osteoporotic vertebral fractures (2,3). However, the only current anabolic agent for osteoporosis treatment available at the moment is Parathyroid hormone (PTH) (either as PTH1-34/ "teriparatide" or full-length PTH1-84). Due to the relatively poor anti-fracture efficacy at some skeletal sites with these current agents, the need for new anabolic targets is paramount. Mechanical loading of bone is widely accepted as a potent anabolic stimulus for bone formation (4) and its use as a preventative measure or treatment for osteoporosis is becoming increasingly attractive (5,6), especially in combination with drugs that target the osteogenic response pathway (7,8). Bone osteogenic adaption to mechanical loading is performed by regulating the activities of both osteoblasts and osteoclasts (9), mediated by the osteocytes and bone lining cells that are thought to act as the principal mechanosensors (10). At the cellular level, mechanical loading-induced osteogenic response is initiate via the release of intracellular molecules such as nitric oxide (NO) and prostaglandins (PG), which are anabolic to osteoblasts (11,12). Mechanical stimuli can also induce extracellular ATP release from a variety of cells, including osteoblasts (13-15). This mechanism is now widely believed to be one of the transduction pathways by which mechanical stimulation initiates a cellular response. Upon stimulation, ATP not only mediates the secretion of other intracellular molecules such as PGs (16), but also activates the purinergic receptors such as the P2X7 receptor which acts as fluid

flow sensor for ATP-dependent phosphorylation of ERK in osteoblasts in vitro (11,17) stimulating proliferation (18). In vivo, P2X7 receptor knockout mice have been shown to have ~70% reduction in the skeletal sensitivity to mechanical loading (19). Other purinergic receptors are activated by extracellular ATP and have been demonstrated to play a role in integrating local and systemic responses in the activation of bone remodelling (20). More recently the $P2Y_{13}$ receptor has been shown to be involved in the regulation of bone remodelling and protection of mice from estrogen deficiency-induced bone loss (21). In addition, the $P2Y_{13}$ receptor was also found to provide a negative feedback pathway to inhibit ATP release from human red blood cells in response to low oxygen level (22). These findings suggest a role for $P2Y_{13}$ receptors in ATP metabolism and potentially in the response to mechanical loading via other purinergic receptor such as the P2X7 receptor. Indeed, there is evidence showing $P2Y_{13}$ and P2X7 receptors co-mediate intracellular calcium responses to BzATP in rat cerebellar astrocytes (23). In addition, it was recently shown that blocking the $P2Y_{13}$ receptor can mediate ERK1/2 involvement in β-cell apoptosis (24). Interestingly, ERK1/2 signalling was demonstrated to be involved in osteoblastic response upon mechanical strain and fluid flow (17,25).

Given the expression of $P2Y_{13}$ receptor by osteoblasts and the observed negative feedback pathway for ATP release in red blood cells, we hypothesised that the $P2Y_{13}$ receptor would play a role in the osteogenic response to mechanical stimulation via regulating ATP metabolism in osteoblasts. To test this hypothesis, we examined the osteogenic response of $P2Y_{13}$ receptor knockout ($P2Y_{13}R^{-/-}$) mice to mechanical stimuli in vivo. Non-invasive controlled axial mechanical loading was performed on left tibiae of 4-month old $P2Y_{13}R^{-/-}$ and wild type (WT) mice in vivo (26,27). Microcomputed tomography (μCT) analysis and dynamic

112 histomorphometry were used to determine the osteogenic response. ATP release and hydrolysis
113 by primary osteoblasts was determined.
114
115 **Materials and Methods**
116 Mice
117 $P2Y_{13}R^{-/-}$ mice (28) were backcrossed onto the C57BL/6J background as previously described.
118 Sixteen week old $P2Y_{13}R^{-/-}$ and WT mice were housed in the same environmentally controlled
119 conditions with a 12hr light/dark cycle at 22°C and free to access 2018 Teklad Global 18%
120 Protein Rodent Diet containing 1.01% Calcium (Harlan Laboratories, UK) and water ad libitum
121 in RB-3 cages. All procedures complied with the UK Animals (Scientific Procedures) Act 1986
122 and were reviewed and approved by the local Research Ethics Committee of the University of
123 Sheffield (Sheffield, UK).
124
125 Mechanical loading in vivo
126 In this study, the non-invasive axial loading tibial model (26) was used to examine responses to
127 mechanical loading in 16 week old WT and $P2Y_{13}R^{-/-}$ mice. The peak load (15N) was selected to
128 induce bone formation in the loaded tibiae since evidence showed that similar peak load can
129 induce osteogenic response in female C57BL/6 mice (26,29,30). Briefly, a 14.5N dynamic load
130 was superimposed onto a 0.5N pre-load at rate of 160,000N/sec. Forty trapezoidal-waveform
131 load cycles (0.2 sec hold at 15N) with 10 sec interval between each cycle were applied to mice
132 tibiae, three times a week for 2 weeks. Mice were injected intraperitoneally with calcein (30
133 mg/kg) on the first (day 1) and last day (day 12) of loading. Mice were then euthanized on day
134 14 (27). Both tibiae were dissected and fixed in 70% ethanol for μCT and dynamic

histomorphometry analysis. The contra-lateral non-loaded limb (right tibia) was treated as internal control for loading [the functional adaption in both cortical and trabecular bone being controlled locally and confined to the loaded bones (27,31)] and the osteogenic responses were expressed as percentage change based on the non-loaded limb data ([Parameters of loaded tibia (left)/ Parameters of own non-loading tibia (right)] x 100%)(32).

μCT

Fixed tibiae were scanned using a SkyScan 1172 desktop μCT machine at a resolution of 4.3μm for the tibia proximal end and 17.3μm for the whole tibia, with the X-ray source operating at 50kV, 200μA and using a 0.5mm aluminium filter. Two-dimensional μCT images were captured and reconstructed by Skyscan NRecon software at threshold of 0.0-0.16 and 0.0-0.14 for tibia proximal end and whole tibia scan respectively. For the tibia proximal end scan, trabecular morphometry was characterized by measuring structural parameters in a 1.0mm thick trabecular region which is 0.2mm below the growth plate. Cortical morphometry was quantified from the cortical regions locating in the proximal 20% (1.0mm thick, 1.0mm below the growth plate) and the midshaft of tibiae (1.0mm thick, 7.0mm below the growth plate). Bone tissue mineral densities (TMD) equal to grams of hydroxylapatite per cube centimetre were calculated based on image greyscale with the following equation: TMD = (0.012 x greyscale value) - 0.296 (21). Nomenclature and symbols were used to describe the μCT derived bone morphometries according to (33).

Linear-elastic finite element analysis (FEA)

Linear-elastic finite element models of the tibiae were generated to simulate compression of the tibia and to verify strains induced by the 15N loading force in representative bones from WT and $P2Y_{13}R^{-/-}$ mice scanned post mortem. Briefly, cement blocks were added to the ends of the tibia to facilitate even application of compressive force at the bone ends. Models were generated directly from voxels of the whole contra-lateral non-loaded tibial μCT scans using a cube-shaped, 8-node brick element with a side length of 0.0349 mm. Isotropic material properties were assigned to the bone elements using the following empirical equations of Somerville et al (34).

$$\rho_{ash} = 0.012\rho_{CT} - 0.296 \quad (\text{in g/cm}^3)$$
$$E = 14.1\rho_{ash} - 2 \quad (\text{in GPa})$$

where ρ_{ash} and ρ_{CT} are ash density and bone density from μCT respectively and E is modulus of elasticity of bone. The modulus of elasticity for cement was assigned to 2 GPa. The Poisson's ratio was set to 0.35 for bone and cement. The models were solved by a commercial FE package ANSYS (ANSYS Inc., Canonsburg, PA, USA) for stress and strain at each element. The loading induced average strain in the cortical and trabecular compartment were calculated on a 1.0 mm in length region, 0.2 mm below the growth plate in tibia. An overall strain through the whole length of the tibia was defined as the compressive displacement derived from the FEA ($L_1 - L'_1$) divided by the original tibial length (L_1) in the non-loading state (Figure 1A).

Bone dynamic histomorphometry

Following μCT analysis, tibiae were embedded into LR White resin (Taab Laboratory Equipment Ltd). Sections were cut (at 10μm) longitudinally using a Leica Microsystems Microtome and were examined under UV illumination using a DMRB microscope (Leica

Microsystems, Milton Keynes, UK). The bone histomorphometry software Osteomeasure (Osteometrics) was used to measure the double labelled surface (dLS), single label surface (sLS), the separation width between the two fluorescent labels (Ir.L.Th), and total bone surface (BS) on a 3-mm length of both endocortical and periosteal surface, 0.25 mm from the growth plate (35). The time separating the two labels (Ir.L.t) was the interval between the two IP injects of calcein and was 12 days in all animals. Based on these measurements, mineralizing surface (MS), mineral apposition rate (MAR), and bone formation rate (BFR/BS) were calculated and reported in the results using nomenclature the based on the report of the ASBMR Histomorphometry Nomenclature Committee (36).

Primary osteoblast isolation

Primary osteoblasts were isolated from neonatal mouse calvariae (less than 72 hours old, 5-7 pups per culture) as described before (21). Calvariae were dissected and the attached soft tissue were digested in 1mg/ml Collagenase 1A (Sigma) for 15 mins. Calvariae were then subjected to serial digestions in 1mg/mL Collagenase 1A for 30 mins; 0.25% Trypsin/EDTA (Gibco) for 15 mins; and 1mg/mL Collagenase 1A for 30 mins, at 37°C. All cells were harvested from the digestion suspensions and seeded into a T75 flask and cultured until confluent in DMEM+GLUTAMAX medium with sodium pyruvate (Gibco), 100 Units/mL Penicillin and 100 μg/mL Streptomycin (Gibco) and 10% foetal bovine serum (FBS) (Gibco).

Endogenous ATP release

Fluid flow-induced shear stress is a known stimulator for endogenous ATP release from cells including osteoblasts (11,16). The mechanical disturbances caused by simple medium

displacement or replacement in vitro are widely accepted methods to induce fluid flow-induced shear stress and stimulate ATP release (37,38) from cells including osteoblasts (39). Therefore medium replacement on primary osteoblast was used to mimic mechanical loading in vitro. First passage primary osteoblasts were seeded into 24 well plates at the density of 5×10^3 cell/well and cultured until 70% confluence in growth medium: DMEM+GLUTAMAX medium with sodium pyruvate (Gibco), 100 Units/mL Penicillin and 100 μg/mL Streptomycin (P/S) (Gibco) and 10% FCS (Gibco). The cells were washed three times with serum free medium: DMEM+GLUTAMAX medium with sodium pyruvate, 100 Units/mL Penicillin and 100 μg/mL Streptomycin, and 25 mM HEPES buffer and replenished with 500μL serum free medium. Samples were collected from four replicate wells at time points 0, 5, 10, 20, 30, 40, 50, and 60 mins. ATP concentration was then determined using the HS ViaLight Kit (Lonza, Slough, UK) as previously described. To confirm that ATP release was not caused by cell death, the cell lysis marker lactate dehydrogenase was measured from non-heat inactivated medium samples using the CytoTox 96 well Non-Radioactive Cytotoxicity Assay (Promega, Southampton, UK) on a SpectraMAX M5e plate reader at 492nm. Samples showing increased LDH release were removed from analysis. Samples for luciferase assay were heated at 98°C for 2 mins to inactivate soluble ATPases and frozen down immediately in liquid nitrogen and stored at -80°C. Samples for LDH Assay were directly frozen down in liquid nitrogen and stored at -80°C.

Exogenous ATP hydrolysis

Following sample collection for endogenous ATP release measurement, the media was removed completely from the wells. Fresh serum free medium (500 μL) was carefully added into each well and the plate incubated for 60 mins at 37°C to return the medium pH and extracellular ATP

concentration to basal levels. Medium samples were collected from four replicate wells per time point for both luciferase and LDH assay prior (t=-1 mins) to the addition of 300nM ATP (Sigma: 99.9% pure by HPLC, reconstituted in 25 mM HEPES buffer) and at time point t=0(immediately after addition), 5, 10, 20, and 30 mins.

Alkaline Phosphatase (ALP) assay

First passage primary osteoblast cells isolated from $P2Y_{13}R^{-/-}$ and WT neonatal calvariae were seeded at $1.5x10^4$ cells per well in a 12-well cell culture plates and cultured for six days. At the end of this time period the cells were washed with PBS and harvested by addition of nuclease-free water into each well and the samples snap frozen at -80°C. Cell lysates were obtained after three freeze thaw cycles. Alkaline Phosphatase (ALP) activity was measured using p-nitrophenyl phosphate (pNPP) (Sigma) as the chromogenic ALP substrate in the presence of Mg^{2+} ions in a buffered solution. The absorbance was read at 405nm using the SpectraMax M5e Microplate Reader. The ALP activity was then normalized to DNA content quantified using Quant-iT™ PicoGreen dsDNA Assay Kit (Invitrogen) according to the manufacturer's instructions.

Statistical analysis

All data are expressed as mean ± SEM. Statistical significance was tested for using either univariate analysis of variance (PASW Statistics, NY) or a t-test (Prism 5,GraphPad, La Jolla).

Results

Osteogenic response of whole tibia

After 2 weeks axial loading of the left tibiae of 16 week-old mice, µCT analysis at the level of the whole bone demonstrated that the loaded tibia of the $P2Y_{13}R^{-/-}$ mice had a significant greater increase in total bone volume (BV) than WT in response to mechanical loading, when compared to the BV of the non-loaded control (126.7% ± 1.2 versus 121.6% ± 1.4, p = 0.0140) (Figure 1 B). The morphological changes were compared on the loaded and non-loaded tibia of WT and $P2Y_{13}R^{-/-}$ mice using µCT 3D models of the whole bone (Figure 1 C). The FEA showed that there was no significant difference in the simulated loading-induced strain through the full length of the tibia between WT and $P2Y_{13}R^{-/-}$ mice (5081 ± 254.4 versus 5048 ± 258.8 microstrain, p = 0.9306) (Figure 1 D). The FEA based average strain across the trabecular (696.0 ± 60.0 versus 693.4 ± 94.5, p = 0.9820) and cortical compartments (757.8 ± 20.3 versus 758.2 ± 20.2, p = 0.9894) were also not significantly different between WT and $P2Y_{13}R^{-/-}$ mice (Figure 1 E, 1 F).

Osteogenic response of trabecular bone

Analysis of the trabecular bone structure of the tibial region by µCT demonstrated that both $P2Y_{13}R^{-/-}$ and WT mice had significantly increased trabecular bone volume (BV/TV), trabecular thickness (Tb.Th), trabecular number (Tb.N),and trabecular pattern factor (Tb.Pf) in loaded tibia compared to internal non-loaded controls. The quantitative data are summarized in Table 1 and thicker trabeculae were clearly visible in images of 3D models of the loaded tibia trabecular bone from both $P2Y_{13}R^{-/-}$ and WT mice (Figure 2 A).

When compared to the parameters from the contra-lateral non-loaded tibia, $P2Y_{13}R^{-/-}$ mice showed a significant higher Tb.Th increase compared to the increase in WT mice (134.1 ± 1.9 % versus 126.3 ± 3.0 %, p = 0.0316) (Figure 2 B), whilst the increase of BV/TV of $P2Y_{13}R^{-/-}$ was

not significantly higher than WT (149.1 ± 5.1 % versus 146.4 ± 4.1 %, p = 0.6982) (Figure 2 C). $P2Y_{13}R^{-/-}$ mice had almost 21% lower Tb.Pf decreases in the loaded tibia (80.1 ± 3.7 % versus 66.2 ± 3.8 %, p = 0.0185) (Figure 2 D). More interestingly, the $P2Y_{13}R^{-/-}$ trabecular bone had positive changes to the structure model index (SMI) compared to negative changes in the WT (107.0 ± 2.8 % versus 95.4 ± 3.7 %, p = 0.0189) (Figure 2 E).

Osteogenic response of cortical bone

Cortical bone volume of the tibia at 20% proximal and at the mid-shaft (Figure 3 A) was measured by μCT and demonstrated that both $P2Y_{13}R^{-/-}$ and WT had significantly increased cortical bone volume (Ct.V) in the loaded tibia (Table 1). Compared to the osteogenic response of WT, $P2Y_{13}R^{-/-}$mice showed significantly greater responses in both regions (Figure 3 B, 3 C), including significantly increased Ct.V response in both the proximal 20% region (136.4 ± 2.3 % versus 128.2 ± 1.5 %, p = 0.0130) (Figure 3 D) and the mid-shaft region (148.3 ± 4.1 % versus 136.6 ± 2.8 %, p = 0.0362) (Figure 3 E).

Rate and extent of mineralization induced by mechanical loading of the tibia

Two distinctive calcein labels (14 and 2 days prior to sacrifice respectively) on both 20% proximal and midshaft endocortical surfaces of tibiae can be visualized using a fluorescent microscope and confirmed the endocortical lamellar bone formation (Figure 4 A). Calcein labels on both endocortical and periosteal surfaces were measured to calculate the parameters including MAR, BFR/BS, and MS. $P2Y_{13}R^{-/-}$ mice showed a significant increase in all three parameters in both endocortical and periosteal surfaces of loaded tibiae, compared to non-loaded control tibiae.

Whilst WT mice only showed significant changes in periosteal BFR/BS and MAR on both periosteal and endocortical surfaces. The quantitative data are summarized in Table 2.

To determine if the response of the $P2Y_{13}R^{-/-}$ mice was different to WT, the loaded tibia data was compared to contra-lateral non-loaded tibia. In the endocortical surfaces, loaded tibia of $P2Y_{13}R^{-/-}$ showed more than a two-fold increased response in MAR (355.4 ± 88.4 % versus 140.5 ± 16.4 %, p = 0.0276) (Figure 4 B), a 5-fold increased response in BFR/BS (714.7 ± 235.4 % versus 171.1 ± 41.1 %, p = 0.0338) (Figure 4 C), and almost a 2-fold higher response in MS (186.6 ± 30.8 % versus 115.6 ± 16.1 %, p = 0.0599) (Figure 4 D). The same trend was found on the periosteal surface, but only the increased response in MAR by $P2Y_{13}R^{-/-}$ mice reached statistical significance (973.7± 108.2 % versus 586.6 ± 116.4 %, p = 0.0402) (Figure 4 E).

Endogenous ATP release from primary osteoblasts in vitro

Endogenous ATP release after medium change from primary osteoblasts was examined using the luciferase assay. LDH assay was used to exclude ATP release due to cell lysis. After medium change (t_0), the initial extracellular ATP released from $P2Y_{13}R^{-/-}$ osteoblasts into the medium showed no significant difference compared to WT cells (18.6nM ± 3.6 versus 20.5nM ± 3.4, p = 0.7063). The extracellular ATP concentration in the medium of WT osteoblast cultures gradually returned to basal level 60 mins (t_{60}) after medium change (t_0 = 20.5nM ± 3.4 versus t_{60} = 9.6nM ± 1.6, p = 0.0227). However, the extracellular ATP concentration in the medium of $P2Y_{13}R^{-/-}$ cells did not return to baseline and demonstrated a trend towards accumulation instead of degradation, with the ATP concentration being significantly higher than the initial concentration from 50 mins onwards (t_0 = 18.6nM ± 3.6 versus t_{50}=32.7nM ± 4.2, p = 0.0182). The extracellular ATP

concentration in the medium of $P2Y_{13}R^{-/-}$ osteoblast cultures was also significantly higher than that of WT cultures from 50 mins after medium change (32.7nM ± 4.2 versus 15.6nM ± 2.6, p = 0.0023) (Figure 5 A).

Exogenous ATP hydrolysis by primary osteoblasts

After measuring endogenous ATP release, primary osteoblast cells were incubated in serum free medium to let ATP concentration and pH settle back to basal levels. Exogenous ATP (300nM) was added into each well and the concentration of ATP in the medium determined over a time course. The hydrolysis of exogenous ATP in $P2Y_{13}R^{-/-}$ osteoblast cultures was slower than that in WT cultures. The ATP concentration in WT osteoblast cultures reduced by 50% within 5 mins, whilst the ATP concentration of $P2Y_{13}R^{-/-}$ cultures was significantly higher than WT from 5 mins and remained at 200 nM level even after 30 mins (Figure 5 B).

ALP activity of primary osteoblasts

ALP is a nucleotidase highly expressed by osteoblasts that is capable of hydrolysing extracellular ATP. The basal level of ALP activity was measured in primary osteoblast cultures using the pNPP assay. $P2Y_{13}R^{-/-}$ mice showed a 15% reduction in ALP activity compared to osteoblasts from WT mice when normalized to DNA content (0.72 ± 0.02 versus 0.85 ± 0.03, p = 0.0002, Figure 5 C).

Discussion

The $P2Y_{13}$ receptor has been suggested to be involved in ATP metabolism in different cell types and ATP release and purinergic signalling is one of the main transduction pathways of

mechanical stimulation. Therefore, we hypothesised that the $P2Y_{13}$ receptor would play a role in regulating ATP metabolism by osteoblasts and in mediating the osteogenic response upon mechanical stimulation. To test this hypothesis, we examined the osteogenic response of $P2Y_{13}R^{-/-}$ mice subject to mechanical stimuli both in vivo and in vitro. The results provide compelling evidence for a role for the $P2Y_{13}R$ in bone homeostasis. Whilst the effect of the deletion of the $P2Y_{13}R$ on the normal bone phenotype is modest, the response to loading in vivo is dramatically enhanced in the KO mice, possibly due to the lack of a $P2Y_{13}R$ regulated negative feedback pathway for ATP release, as demonstrated in vitro**.**

Non-invasive axial mechanical loading at peak loading force of 15N was performed on left tibiae of both $P2Y_{13}R^{-/-}$ and WT mice in vivo using a method as described before (26,27). Compared to the contra-lateral non-loaded right tibia, the total bone volume of loaded tibia demonstrated significant increases in both WT and $P2Y_{13}R^{-/-}$ mice although bone length did not change. This indicated that mechanical loading successfully induced osteogenic response mainly in the tibia cross-sectional dimensions (40). High resolution μCT analysis showed that trabecular bone in both WT and $P2Y_{13}R^{-/-}$ loaded tibia had significantly increased BV/TV, Tb.Th and Tb.N. Similar increases in Ct.V were also found in cortical bone. Therefore, the total BV increase was a combined result of new bone formation activities from both trabecular and cortical bone. This was confirmed with the increased BFR and MAR in both WT and $P2Y_{13}R^{-/-}$ loaded tibiae using dynamic histomorphometry analysis, especially the lamellar bone formation on the endocortical bone surfaces. In addition, increased bone remodeling activities led to coarse surface which was observed specifically in the periosteal surface of tibial proximal end 3D μCT image. This result was consistent with previous findings that there was a greater osteogenic response in the

362 corticocancellous proximal metaphysis (41) and periosteal formation surface was predominantly
363 woven bone (42,43).
364
365 To compare the extent of the osteogenic response between $P2Y_{13}R^{-/-}$ and WT mice, the
366 parameters from loaded tibia were compared to those from the corresponding contra-lateral non-
367 loaded tibia controls. The $P2Y_{13}R^{-/-}$ mice had a further 20% response in total BV increase in the
368 loaded tibiae compared to WT. This was mainly the result of the increased osteogenic response
369 of cortical bone because $P2Y_{13}R^{-/-}$ had a significant greater response in the increases in Ct.V but
370 not in trabecular BV/TV over that of WT. The higher osteogenic response in $P2Y_{13}R^{-/-}$ mice
371 under mechanical stimulation mainly involved osteoblastic bone forming activities. This was
372 confirmed by the results of fluorochrome double labelling in the cortical compartment which
373 showed dramatically higher MAR and BFR increases in $P2Y_{13}R^{-/-}$ bones compared to WT,
374 indicate enhanced activities of osteoblasts (36).
375
376 The trabecular structure of $P2Y_{13}R^{-/-}$ mice after loading did not alter towards the ideal load
377 bearing architecture as the WT mice did; the $P2Y_{13}R^{-/-}$ mice showed less of a decrease in Tb.Pf
378 and significantly increased SMI, indicating that the trabecular did not improve connectivity in
379 any great extent and remained a rod-like structure (44,45). However, WT mice showed better
380 structure alteration with significantly decreased Tb.Pf and slightly reduced SMI. The reduced
381 change in Tb.Pf could be the result of a weaker primary trabecular structure in $P2Y_{13}R^{-/-}$ bones,
382 whereas, the possible reason for an increased SMI could be due to a failure in osteoclast
383 resorption of the $P2Y_{13}R^{-/-}$ mice as demonstrated previously (21). This would lead to an

abnormal capacity to remodel the trabecular structure since osteoclasts are suggested to control the conversion of trabecular from plate elements to rod elements (45).

One possible explanation for the different osteogenic response could have been that the lower bone volume in the $P2Y_{13}R^{-/-}$ mice led to an increase in the strains engendered by the 15N loading. However, our FEA studies, a widely recognized method to predict loading induced strain (46), demonstrated that this is not the case because the bones of the WT and $P2Y_{13}R^{-/-}$ mice experienced the same overall strains and average strain across trabecular and cortical compartments under modelled loading. The overall strains calculated were in the region of 5,000 microstrain and are relatively higher than previous studies using strain gauge to measure strain (26,27,30) but are consistent with other new findings using FEA (43). This is because applying the 15N loads to the tibia in silico is not the same as loading tibia in vivo, where several layers of other tissues including skin, subcutaneous tissues, and at least two thicknesses of cartilage are compressed as well. The important issue is therefore not the absolute values derived from the FEA measurement but the lack of strain difference between WT and $P2Y_{13}R^{-/-}$ bones and hence the observed enhanced osteogenic response to mechanical loading in $P2Y_{13}R^{-/-}$ mice is real.

Another possible cause of the different osteogenic response could have been the result of enhanced woven bone formation due to an increased inflammatory response (47). However, our dynamic histomorphometry results clearly show lamellar bone formation on the endocortical bone surface, where the increases in both MAR and BFR/BS in loaded tibiae were significantly higher in $P2Y_{13}R^{-/-}$ than those in WT mice. On the periosteal surface, where woven bone formation was predominant, there is a similar trend of enhanced bone formation in $P2Y_{13}R^{-/-}$

mice but it is not as dramatic as on the endocortical bone surfaces and only the MAR reached statistical significance at this site. Therefore, there may be an element of an inflammatory response but we believe it is not the main cause of the different adaption to mechanical loading between WT and $P2Y_{13}R^{-/-}$ mice.

Many mechanisms has been suggested to be involved in the alteration of osteogenic response to mechanical loading in mice, including aging and changes in other signalling pathways such as Wnt, ER and BMP/TGFβ pathways (48,49). The in vitro findings in this study may provide a possible explanation for the reason why $P2Y_{13}R^{-/-}$ mice had enhanced osteogenic response to mechanical loading. The constitutive endogenous ATP release was investigated in the primary osteoblasts isolated from neonatal mice calvariae using luciferase assay. After medium change, the extracellular ATP concentration in the medium of $P2Y_{13}R^{-/-}$ osteoblast cultures showed a trend towards accumulation of ATP instead of gradually degrading ATP as in WT osteoblast cultures. As a result, $P2Y_{13}R^{-/-}$ osteoblasts showed three fold higher extracellular ATP concentration than WT cells one hour after medium change. This confirms that the deletion of $P2Y_{13}R$ results in a lack of the negative feedback pathway for ATP release in $P2Y_{13}R^{-/-}$ osteoblasts. Interestingly, when a higher concentration of exogenous ATP was added to the primary osteoblasts, $P2Y_{13}R^{-/-}$ cells have a decreased capacity to hydrolyse ATP, whilst WT osteoblasts degraded the exogenous ATP back to basal levels within 5 minutes. Thirty minutes after exogenous ATP treatment, extracellular ATP concentration of $P2Y_{13}R^{-/-}$ osteoblasts was double that of WT cells. Osteoblasts are known to have numerous membrane-bound nucleotidases which are responsible for breaking down ATP to adenosine and are critical in the ATP turnover process (50). One particular nucleotidase, ALP, is highly expressed by osteoblasts

and interestingly, the ALP activity in vitro was found to be 15% lower in $P2Y_{13}R^{-/-}$ osteoblasts than WT under basal conditions, possibly due to the down regulation of RhoA/ROCK I signalling pathway as a consequence of $P2Y_{13}R$ deletion (21,51). Therefore, one possible mechanism leading to the observed higher osteogenic response to mechanical loading in $P2Y_{13}R^{-/-}$ mice may be as a result of a reduction in nucleotidase activity. Under basal conditions, it appears that the reduced level of ATP hydrolysis to ADP is still sufficient to provide a negative feedback pathway to regulate ATP release. However, under mechanical stimulation, increased and sustained ATP release may not be matched by hydrolysis to ADP due to basal reduced ALP levels, and therefore a lack of the negative feedback loop leads to extracellular ATP accumulation. This extracellular ATP accumulation may in turn trigger other P2 receptor signalling pathways and cause an increased osteogenic response possibly via ATP-dependent phosphorylation of ERK (11,17), which then stimulates osteoblastic proliferation and drives the osteogenic response (18).

In conclusion, this study examined the role of $P2Y_{13}$ receptor in bone osteogenic response to mechanical loading in vivo and in vitro. Deletion of the $P2Y_{13}R$ leads to higher bone formation, mainly in cortical compartment, than WT upon mechanical loading in vivo, possibly due to the lack of $P2Y_{13}R$ regulated negative feedback pathway for ATP release. This was further supported by our in vitro findings of abnormal extracellular ATP accumulation from primary osteoblast under mechanical stimulation. Reduced ALP activity caused by $P2Y_{13}R$ gene deletion and the following reduction in extracellular ATP degradation might be one reason for this phenomenon. This augmented osteogenic response to mechanical stimulation, combined with suppressed bone remodelling activities and protect from OVX induced bone loss after $P2Y_{13}R$

453 depletion as recently described (21), suggests a potential role for $P2Y_{13}R$ antagonist-based
454 therapy, possibly in combination with mechanical loading, for the treatment of osteoporosis in
455 the future.
456
457 **Acknowledgements**
458 The authors would like to thank the staff of the Bone Analysis Laboratory, The University of
459 Sheffield for tissues processing. This study was supported by the European Commission under
460 the 7th Framework Programme (proposal #202231) performed as a collaborative project among
461 the members of the ATPBone Consortium (Copenhagen University, University College London,
462 University of Maastricht, University of Ferrara, University of Liverpool, University of Sheffield,
463 and Université Libre de Bruxelles), and is a sub study under the main study "Fighting
464 osteoporosis by blocking nucleotides: purinergic signalling in bone formation and homeostasis".
465
466 **Authors' roles:** AG, TS and JMB conceived the project. NW and RR performed the experiments.
467 NW and LY performed the FEA. BR generated the $P2Y_{13}R^{-/-}$ mice. Data analysis and
468 interpretation: NW, RR, LY, TS, JMB and AG. NW and AG wrote the draft manuscript, with
469 input from all authors.
470

References:

1. Cooper C 2003 Epidemiology of Osteoporosis. In: Favus M (ed.) Primer on the Metabolic Bone Diseases and Disorders of Mineral Metabolism. American Society for Bone and Mineral Research, Washington, DC, pp 307-313.
2. Russell RG, Xia Z, Dunford JE, Oppermann U, Kwaasi A, Hulley PA, Kavanagh KL, Triffitt JT, Lundy MW, Phipps RJ, Barnett BL, Coxon FP, Rogers MJ, Watts NB, Ebetino FH 2007 Bisphosphonates: an update on mechanisms of action and how these relate to clinical efficacy. Ann N Y Acad Sci **1117:**209-57.
3. McClung M, Boonen S, Torring O, Roux C, Rizzoli R, Bone H, Benhamou CL, Lems W, Minisola S, Halse J, Hoeck H, Eastell R, Wang A, Siddhanti S, Cummings S 2012 Effect of denosumab treatment on the risk of fractures in subgroups of women with postmenopausal osteoporosis. J Bone Miner Res **27**(1)**:**211-218.
4. Turner CH, Owan I, Alvey T, Hulman J, Hock JM 1998 Recruitment and proliferative responses of osteoblasts after mechanical loading in vivo determined using sustained-release bromodeoxyuridine. Bone **22**(5)**:**463-9.
5. Galloway MT, Jokl P 2000 Aging successfully: the importance of physical activity in maintaining health and function. J Am Acad Orthop Surg **8**(1)**:**37-44.
6. Rubin C, Turner AS, Bain S, Mallinckrodt C, McLeod K 2001 Anabolism. Low mechanical signals strengthen long bones. Nature **412**(6847)**:**603-4.
7. Braith RW, Magyari PM, Fulton MN, Aranda J, Walker T, Hill JA 2003 Resistance exercise training and alendronate reverse glucocorticoid-induced osteoporosis in heart transplant recipients. J Heart Lung Transplant **22**(10)**:**1082-90.
8. Braith RW, Conner JA, Fulton MN, Lisor CF, Casey DP, Howe KS, Baz MA 2007 Comparison of alendronate vs alendronate plus mechanical loading as prophylaxis for osteoporosis in lung transplant recipients: a pilot study. J Heart Lung Transpl **26**(2)**:**132-137.
9. Noble BS, Peet N, Stevens HY, Brabbs A, Mosley JR, Reilly GC, Reeve J, Skerry TM, Lanyon LE 2003 Mechanical loading: biphasic osteocyte survival and targeting of osteoclasts for bone destruction in rat cortical bone. Am J Physiol Cell Physiol **284**(4)**:**C934-43.
10. Skerry TM, Bitensky L, Chayen J, Lanyon LE 1989 Early strain-related changes in enzyme activity in osteocytes following bone loading in vivo. J Bone Miner Res **4**(5)**:**783-8.
11. Liu D, Genetos DC, Shao Y, Geist DJ, Li J, Ke HZ, Turner CH, Duncan RL 2008 Activation of extracellular-signal regulated kinase (ERK1/2) by fluid shear is Ca(2+)-and ATP-dependent in MC3T3-E1 osteoblasts. Bone **42**(4)**:**644-52.
12. Burger EH, Klein-Nulen J 1999 Responses of bone cells to biomechanical forces in vitro. Adv Dent Res **13:**93-8.
13. Romanello M, Pani B, Bicego M, D'Andrea P 2001 Mechanically induced ATP release from human osteoblastic cells. Biochem Biophys Res Commun **289**(5)**:**1275-81.
14. Romanello M, Codognotto A, Bicego M, Pines A, Tell G, D'Andrea P 2005 Autocrine/paracrine stimulation of purinergic receptors in osteoblasts: contribution of vesicular ATP release. Biochem Biophys Res Commun **331**(4)**:**1429-38.
15. Rumney RM, Sunters A, Reilly GC, Gartland A 2012 Application of multiple forms of mechanical loading to human osteoblasts reveals increased ATP release in response to

fluid flow in 3D cultures and differential regulation of immediate early genes. J. Biomech. **45**(3)**:**549-54.
16. Genetos DC, Geist DJ, Liu D, Donahue HJ, Duncan RL 2005 Fluid shear-induced ATP secretion mediates prostaglandin release in MC3T3-E1 osteoblasts. J Bone Miner Res **20**(1)**:**41-9.
17. Okumura H, Shiba D, Kubo T, Yokoyama T 2008 P2X7 receptor as sensitive flow sensor for ERK activation in osteoblasts. Biochem Biophys Res Commun **372**(3)**:**486-90.
18. Jiang GL, White CR, Stevens HY, Frangos JA 2002 Temporal gradients in shear stimulate osteoblastic proliferation via ERK1/2 and retinoblastoma protein. Am J Physiol Endocrinol Metab **283**(2)**:**E383-9.
19. Li J, Liu D, Ke HZ, Duncan RL, Turner CH 2005 The P2X7 nucleotide receptor mediates skeletal mechanotransduction. J Biol Chem **280**(52)**:**42952-9.
20. Bowler WB, Buckley KA, Gartland A, Hipskind RA, Bilbe G, Gallagher JA 2001 Extracellular nucleotide signaling: a mechanism for integrating local and systemic responses in the activation of bone remodeling. Bone **28**(5)**:**507-12.
21. Wang N, Robaye B, Agrawal A, Skerry TM, Boeynaems JM, Gartland A 2012 Reduced bone turnover in mice lacking the P2Y(13) receptor of ADP. Mol Endocrinol **26**(1)**:**142-52.
22. Wang L, Olivecrona G, Gotberg M, Olsson ML, Winzell MS, Erlinge D 2005 ADP acting on P2Y13 receptors is a negative feedback pathway for ATP release from human red blood cells. Circ Res **96**(2)**:**189-96.
23. Carrasquero LM, Delicado EG, Bustillo D, Gutierrez-Martin Y, Artalejo AR, Miras-Portugal MT 2009 P2X7 and P2Y13 purinergic receptors mediate intracellular calcium responses to BzATP in rat cerebellar astrocytes. J Neurochem **110**(3)**:**879-89.
24. Tan C, Salehi A, Svensson S, Olde B, Erlinge D 2010 ADP receptor P2Y(13) induce apoptosis in pancreatic beta-cells. Cell Mol Life Sci **67**(3)**:**445-53.
25. Jessop HL, Rawlinson SC, Pitsillides AA, Lanyon LE 2002 Mechanical strain and fluid movement both activate extracellular regulated kinase (ERK) in osteoblast-like cells but via different signaling pathways. Bone **31**(1)**:**186-94.
26. De Souza RL, Matsuura M, Eckstein F, Rawlinson SC, Lanyon LE, Pitsillides AA 2005 Non-invasive axial loading of mouse tibiae increases cortical bone formation and modifies trabecular organization: a new model to study cortical and cancellous compartments in a single loaded element. Bone **37**(6)**:**810-8.
27. Sugiyama T, Price JS, Lanyon LE 2010 Functional adaptation to mechanical loading in both cortical and cancellous bone is controlled locally and is confined to the loaded bones. Bone **46**(2)**:**314-21.
28. Fabre AC, Malaval C, Ben Addi A, Verdier C, Pons V, Serhan N, Lichtenstein L, Combes G, Huby T, Briand F, Collet X, Nijstad N, Tietge UJ, Robaye B, Perret B, Boeynaems JM, Martinez LO 2010 P2Y13 receptor is critical for reverse cholesterol transport. Hepatology **52**(4)**:**1477-83.
29. Moustafa A, Sugiyama T, Saxon LK, Zaman G, Sunters A, Armstrong VJ, Javaheri B, Lanyon LE, Price JS 2009 The mouse fibula as a suitable bone for the study of functional adaptation to mechanical loading. Bone **44**(5)**:**930-5.
30. Sugiyama T, Saxon LK, Zaman G, Moustafa A, Sunters A, Price JS, Lanyon LE 2008 Mechanical loading enhances the anabolic effects of intermittent parathyroid hormone (1-34) on trabecular and cortical bone in mice. Bone **43**(2)**:**238-48.

562 31. De Souza RL, Pitsillides AA, Lanyon LE, Skerry TM, Chenu C 2005 Sympathetic
563 nervous system does not mediate the load-induced cortical new bone formation. J Bone
564 Miner Res **20**(12)**:**2159-68.
565 32. Windahl S, Saxon L, Borjesson A, Lagerquist M, Frenkel B, Henning P, Lerner U, Galea
566 G, Meakin L, Engdahl C, Sjogren K, Antal M, Krust A, Chambon P, Lanyon L, Price J,
567 Ohlsson C 2012 Estrogen receptor-alpha is required for the osteogenic response to
568 mechanical loading in a ligand-independent manner involving its activation function 1
569 but not 2. J Bone Miner Res. Sep 12. doi: 10.1002/jbmr.1754.
570 33. Bouxsein ML, Boyd SK, Christiansen BA, Guldberg RE, Jepsen KJ, Muller R 2010
571 Guidelines for assessment of bone microstructure in rodents using micro-computed
572 tomography. J Bone Miner Res **25**(7)**:**1468-86.
573 34. Somerville JM, Aspden RM, Armour KE, Armour KJ, Reid DM 2004 Growth of
574 C57BL/6 mice and the material and mechanical properties of cortical bone from the tibia.
575 Calcif Tissue Int **74**(5)**:**469-75.
576 35. Heath DJ, Chantry AD, Buckle CH, Coulton L, Shaughnessy JD, Jr., Evans HR,
577 Snowden JA, Stover DR, Vanderkerken K, Croucher PI 2009 Inhibiting Dickkopf-1
578 (Dkk1) removes suppression of bone formation and prevents the development of
579 osteolytic bone disease in multiple myeloma. J Bone Miner Res **24**(3)**:**425-36.
580 36. Parfitt AM, Drezner MK, Glorieux FH, Kanis JA, Malluche H, Meunier PJ, Ott SM,
581 Recker RR 1987 Bone histomorphometry: standardization of nomenclature, symbols, and
582 units. Report of the ASBMR Histomorphometry Nomenclature Committee. J Bone Miner
583 Res **2**(6)**:**595-610.
584 37. Lazarowski ER, Boucher RC, Harden TK 2000 Constitutive release of ATP and evidence
585 for major contribution of ecto-nucleotide pyrophosphatase and nucleoside
586 diphosphokinase to extracellular nucleotide concentrations. J Biol Chem **275**(40)**:**31061-
587 8.
588 38. Okada SF, O'Neal WK, Huang P, Nicholas RA, Ostrowski LE, Craigen WJ, Lazarowski
589 ER, Boucher RC 2004 Voltage-dependent anion channel-1 (VDAC-1) contributes to ATP
590 release and cell volume regulation in murine cells. J. Gen. Physiol. **124**(5)**:**513-26.
591 39. Orriss IR, Knight GE, Utting JC, Taylor SE, Burnstock G, Arnett TR 2009 Hypoxia
592 stimulates vesicular ATP release from rat osteoblasts. J Cell Physiol **220**(1)**:**155-62.
593 40. Wallace JM, Rajachar RM, Allen MR, Bloomfield SA, Robey PG, Young MF, Kohn DH
594 2007 Exercise-induced changes in the cortical bone of growing mice are bone- and
595 gender-specific. Bone **40**(4)**:**1120-7.
596 41. Fritton JC, Myers ER, Wright TM, van der Meulen MC 2005 Loading induces site-
597 specific increases in mineral content assessed by microcomputed tomography of the
598 mouse tibia. Bone **36**(6)**:**1030-8.
599 42. Akhter MP, Cullen DM, Pedersen EA, Kimmel DB, Recker RR 1998 Bone response to in
600 vivo mechanical loading in two breeds of mice. Calcif Tissue Int **63**(5)**:**442-9.
601 43. Sugiyama T, Meakin LB, Browne WJ, Galea GL, Price JS, Lanyon LE 2012 Bones'
602 adaptive response to mechanical loading is essentially linear between the low strains
603 associated with disuse and the high strains associated with the lamellar/woven bone
604 transition. J. Bone Miner. Res. **27**(8)**:**1784-93.
605 44. Hahn M, Vogel M, Pompesius-Kempa M, Delling G 1992 Trabecular bone pattern
606 factor--a new parameter for simple quantification of bone microarchitecture. Bone
607 **13**(4)**:**327-30.

45. Hildebrand T, Ruegsegger P 1997 Quantification of Bone Microarchitecture with the Structure Model Index. Comput Methods Biomech Biomed Engin **1**(1)**:**15-23.
46. Silva MJ, Brodt MD, Hucker WJ 2005 Finite element analysis of the mouse tibia: estimating endocortical strain during three-point bending in SAMP6 osteoporotic mice. Anat Rec A Discov Mol Cell Evol Biol **283**(2)**:**380-90.
47. McKenzie JA, Bixby EC, Silva MJ 2011 Differential gene expression from microarray analysis distinguishes woven and lamellar bone formation in the rat ulna following mechanical loading. PLoS One **6**(12)**:**e29328.
48. Kapur S, Mohan S, Baylink DJ, Lau KH 2005 Fluid shear stress synergizes with insulin-like growth factor-I (IGF-I) on osteoblast proliferation through integrin-dependent activation of IGF-I mitogenic signaling pathway. J Biol Chem **280**(20)**:**20163-70.
49. Saxon LK, Robling AG, Castillo AB, Mohan S, Turner CH 2007 The skeletal responsiveness to mechanical loading is enhanced in mice with a null mutation in estrogen receptor-beta. Am J Physiol Endocrinol Metab **293**(2)**:**E484-91.
50. Yegutkin GG 2008 Nucleotide- and nucleoside-converting ectoenzymes: Important modulators of purinergic signalling cascade. Biochim Biophys Acta **1783**(5)**:**673-94.
51. Khatiwala CB, Kim PD, Peyton SR, Putnam AJ 2009 ECM compliance regulates osteogenesis by influencing MAPK signaling downstream of RhoA and ROCK. J Bone Miner Res **24**(5)**:**886-98.

Tables

Table 1. Quantitative results of tibia trabecular and cortical bone after mechanical loading using µCT analysis.

	WT **n=9**			**$P2Y_{13}R^{-/-}$** **n=12**		
	Loaded	Non-loaded	p value	Loaded	Non-loaded	p value
TMD (g/cm^3)	1.12 ± 0.00	1.13 ± 0.01	b	1.12 ± 0.00	1.13 ± 0.00	a
BV/TV	12.30 ± 0.39	8.42 ± 0.19	c	8.60 ± 0.37	5.80 ± 0.24	c
BS/BV (1/mm)	65.00 ± 1.05	85.41 ± 1.33	c	67.80 ± 0.60	91.50 ± 1.24	c
Tb.Th (mm)	0.064 ± 0.001	0.051 ± 0.001	c	0.065 ± 0.001	0.048 ± 0.001	c
Tb.N (1/mm)	1.93 ± 0.07	1.66 ± 0.04	a	1.33 ± 0.06	1.20 ± 0.05	a
Tb.Pf (1/mm)	16.93 ± 0.95	25.62 ± 0.57	c	24.38 ± 0.89	30.72 ± 0.94	c
Tb.Sp (mm)	0.25 ± 0.01	0.26 ± 0.01		0.29 ± 0.01	0.31 ± 0.01	
SMI	2.06 ± 0.06	2.16 ± 0.03		2.53 ± 0.05	2.37 ± 0.05	a
DA	2.04 ± 0.08	2.28 ± 0.10		1.66 ± 0.05	1.90 ± 0.06	a
Proximal 20% Ct.V (mm3)	1.16 ± 0.02	0.91 ± 0.01	c	1.17 ± 0.02	0.86 ± 0.01	c
Midshaft Ct.V (mm3)	0.98 ± 0.02	0.71 ± 0.01	c	1.00 ± 0.02	0.67 ± 0.01	c

Values are mean ± SEM, [a] $p < 0.05$, [b] $p < 0.01$, [c] $p < 0.001$ (paired t-test)

Table 2. Quantitative results of endocortical and periosteal tibia dynamic histomorphometry.

	WT			**$P2Y_{13}R^{-/-}$**		
	n=6			**n=5**		
	Loaded	Non-loaded	p value	Loaded	Non-loaded	p value
Endocortical MS (%)	85.68 ± 6.26	78.20 ± 6.85		88.83 ± 0.87	51.97 ± 6.77	b
Endocortical MAR (µm/day)	1.87 ± 0.16	1.38 ± 0.11	a	2.60 ± 0.59	0.80 ± 0.15	a
Endocortical BFR/BS ($\mu m^3/ \mu m^2$/day)	1.58 ± 0.14	1.11± 0.16		2.32 ± 0.55	0.44 ± 0.13	a
Periosteal MS (%)	94.91 ± 3.47	78.83 ± 11.01		92.09 ± 3.71	52.53 ± 9.12	b
Periosteal MAR (µm/day)	3.62 ± 0.56	0.65 ± 0.06	b	3.28 ± 0.39	0.34 ± 0.03	b
Periosteal BFR/BS ($\mu m^3/ \mu m^2$/day)	3.45 ± 0.57	0.54 ± 0.01	b	3.05 ± 0.42	0.19 ± 0.05	b

Values are mean ± SEM,[a] $p < 0.05$,[b] $p < 0.01$,[c] $p < 0.001$ (paired t-test)

Legends

Figure 1 Whole bone response to mechanical loading

(A) Finite element models of the mice tibia showing the loading and constraint conditions and length changes before (L_1) and under compressive load (L'_1). **(B)** Percentage change in whole tibial bone volume of the loaded compared to unloaded internal control. All values are mean ± SEM, $P2Y_{13}R^{-/-}$ n=12; WT n=9. [a] $p<0.05$ (unpaired t-test). **(C)** The 3D models of whole tibia from $P2Y_{13}R^{-/-}$ and WT loaded and non-loaded animals were constructed from µCT images, scale bar = 2.0mm. **(D)** The overall strain based on compressive displacement of the whole tibia was analysed by FEA and compared between WT and $P2Y_{13}R^{-/-}$**.** The average strain in the **(E)** trabecular and **(F)** cortical compartment were also calculated from a 1.0 mm in length region, 0.2 mm below the growth plate in tibia. n=5 (unpaired t-test).

Figure 2. Trabecular bone response to mechanical loading

(A) Three dimensional images of a region of 1.0mm thick trabecular bone 0.2mm below the growth plate of mechanical loaded and non-loaded tibiae, scale bar = 0.5 mm. The contra-lateral non-loaded right tibiae were used as internal controls. The percentage change of **(B)** trabecular thickness **(**Tb.Th), **(C)** trabecular bone volume (BV/TV), **(D)** trabecular pattern factor (Tb.Pf), and **(E)** structure model index (SMI) for loaded tibia compared to unloaded controls. All values are mean ± SEM, $P2Y_{13}R^{-/-}$ n=12; WT n=9. [a] $p<0.05$ (unpaired t-test).

Figure 3. Cortical bone response to mechanical loading.

(A) Mouse tibial 3D models indicating the two regions analysed for determining cortical bone parameters, including proximal 20% and the mid-shaft of tibiae (1.0mm in thickness, 1.0mm and

7.0mm below the growth plate respectively). The cross section μCT images of loaded and non-loaded tibiae were compared between WT and $P2Y_{13}R^{-/-}$ at **(B)** 2.0mm and **(C)** 8.0mm below the growth plate. The Ct.V in loaded tibiae normalized to contra-lateral non-loaded right tibiae at **(D)** the proximal 20% region and **(E)** the mid-shaft region. All values are mean ± SEM, $P2Y_{13}R^{-/-}$ n=12; WT n=9. [a] $p<0.05$ (unpaired t-test).

Figure 4. Rate and extent of mineralization induced by mechanical loading of the tibia

Double calcein labelling was used to determine the bone formation activities on both endocortical and periosteal surface. **(A)** Clear double labelling of calcein on endocortical surfaces confirmed lamellar bone formation at this site. The percentage change of loaded tibia compared to contra-lateral non-loaded right tibiae of **(B)** Mineral apposition rate (MAR), **(C)** bone formation rate **(**BFR/BS), and **(D)** mineralizing surface (MS%) on the endocortical surface. **(E)** MAR, **(F)** BFR/BS, and **(G)** MS on the periosteal surface. All values are mean ± SEM, $P2Y_{13}R^{-/-}$ n = 5, WT n = 6, [a] $p<0.05$ (unpaired t-test).

Figure 5. Regulation of extracellular ATP levels in osteoblast cultures.

(A) A time course of ATP release and degradation in osteoblast cultures following medium change. $P2Y_{13}R^{-/-}$ osteoblasts showed a trend of extracellular ATP accumulation compared to the gradual degradation seen in WT cultures. All values are mean ± SEM, n = 4 per experiment, with 3 independent experiments, [a] $p<0.05$, [b] $p<0.01$ (unpaired t-test). **(B)** Exogenous ATP (300nM) was hydrolyzed to half the amount within 5 mins in WT osteoblast cultures. However, the degradation of exogenous ATP in $P2Y_{13}R^{-/-}$ osteoblasts was slower than WT, with extracellular ATP concentration in the $P2Y_{13}R^{-/-}$ cultures being significantly higher than WT from 5 mins

onwards. All values are mean ± SEM, n = 4 per experiment, with 3 independent experiments, [b] $p<0.01$, [c] $p<0.001$ (unpaired t-test). **(C)** ALP activity of WT and $P2Y_{13}R^{-/-}$ osteoblast cultures was measured using pNPP assay and normalized to dsDNA content. All values are mean ± SEM, n=3 repeat experiments with 12 replicates per experiment, [c] $p < 0.001$, (Univariate analysis of variance).

Figure 1

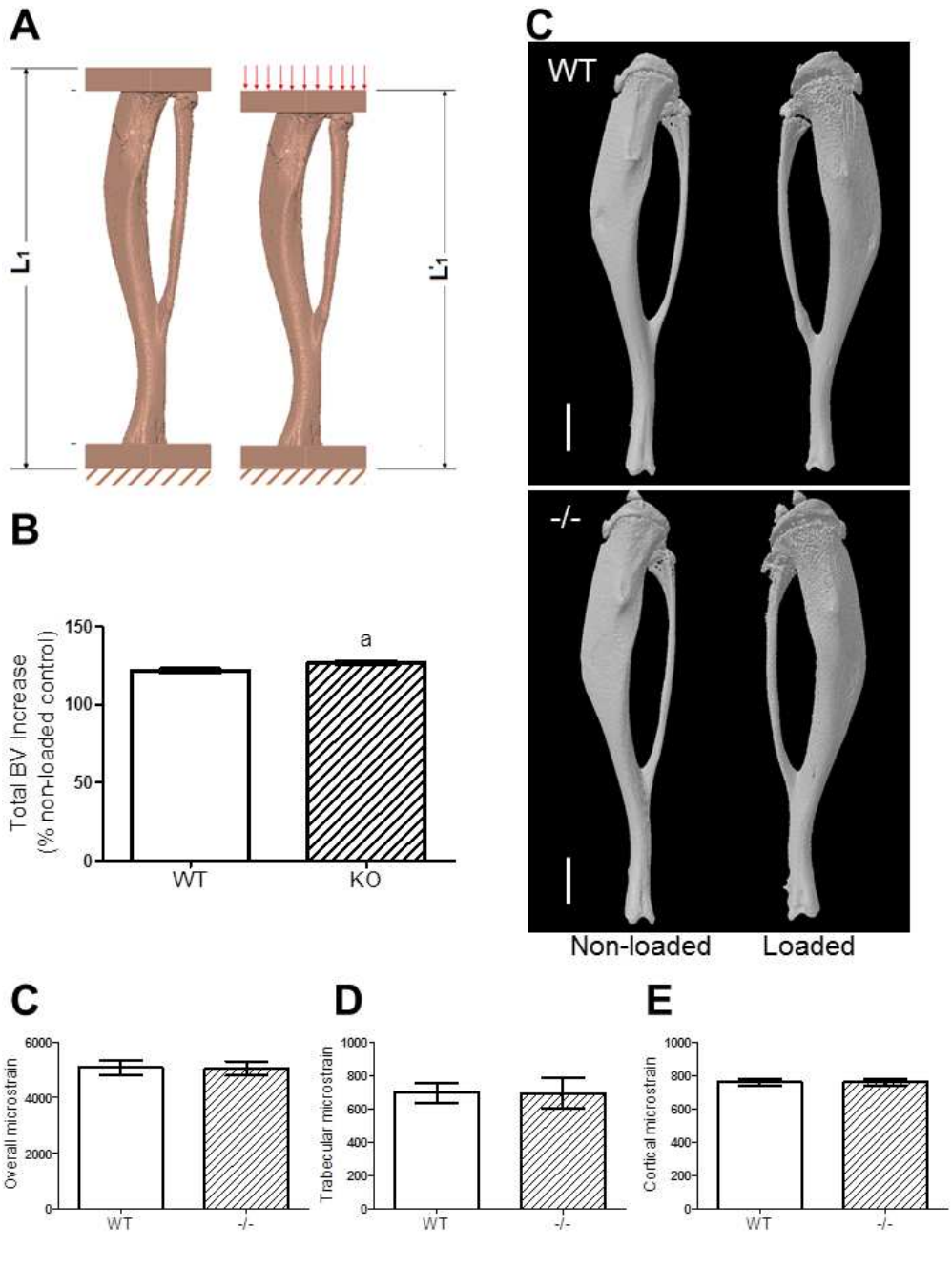
A
L1
L'1
B
Total BV Increase
(% non-loaded control)
150
100
50
0
a
WT
KO
C
WT
-/-
Non-loaded
Loaded
C
Overall microstrain
6000
4000
2000
0
WT
-/-
D
Trabecular microstrain
1000
800
600
400
200
0
WT
-/-
E
Cortical microstrain
1000
800
600
400
200
0
WT
-/-

Figure 2

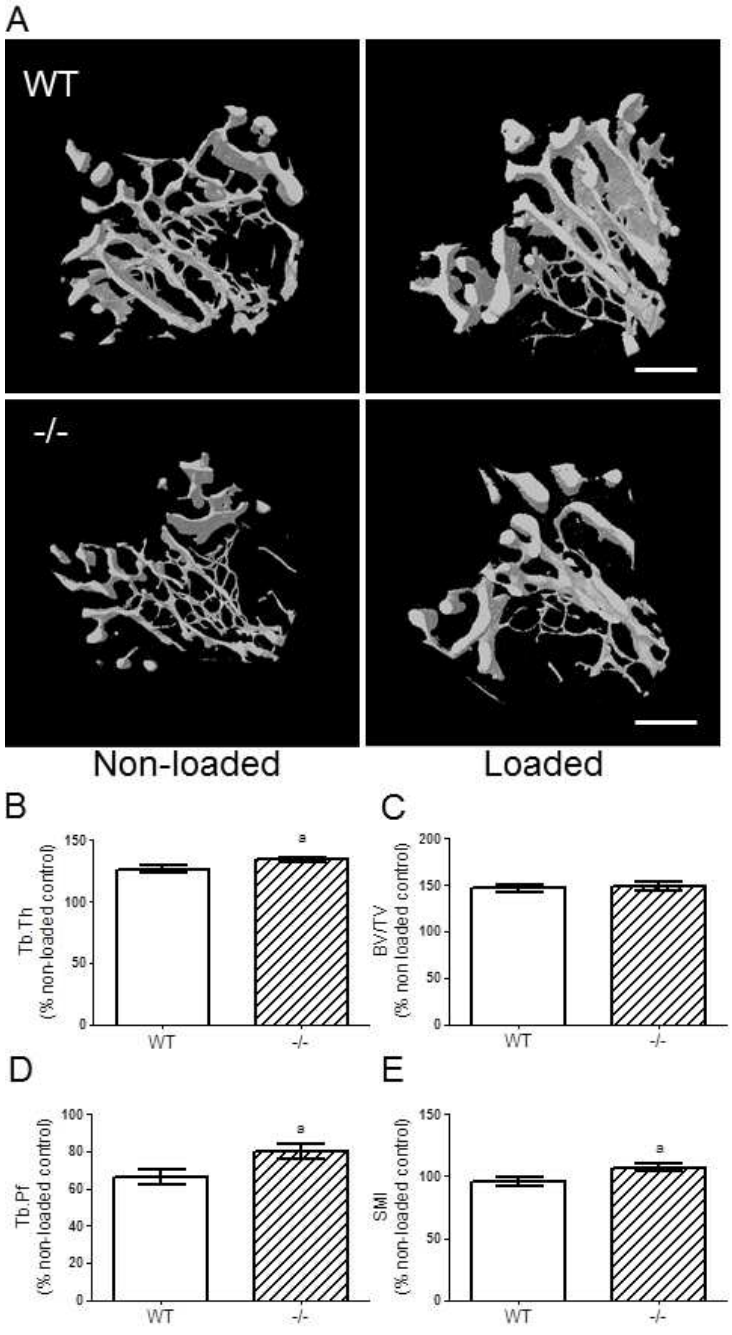
A
WT
-/-
Non-loaded
Loaded
B
Tb.Th
(% non-loaded control)
150
100
50
0
a
WT
-/-
C
BV/TV
(% non loaded control)
200
150
100
50
0
WT
-/-
D
Tb.Pf
(% non-loaded control)
100
80
60
40
20
0
a
WT
-/-
E
SMI
(% non-loaded control)
150
100
50
0
a
WT
-/-

Figure 3

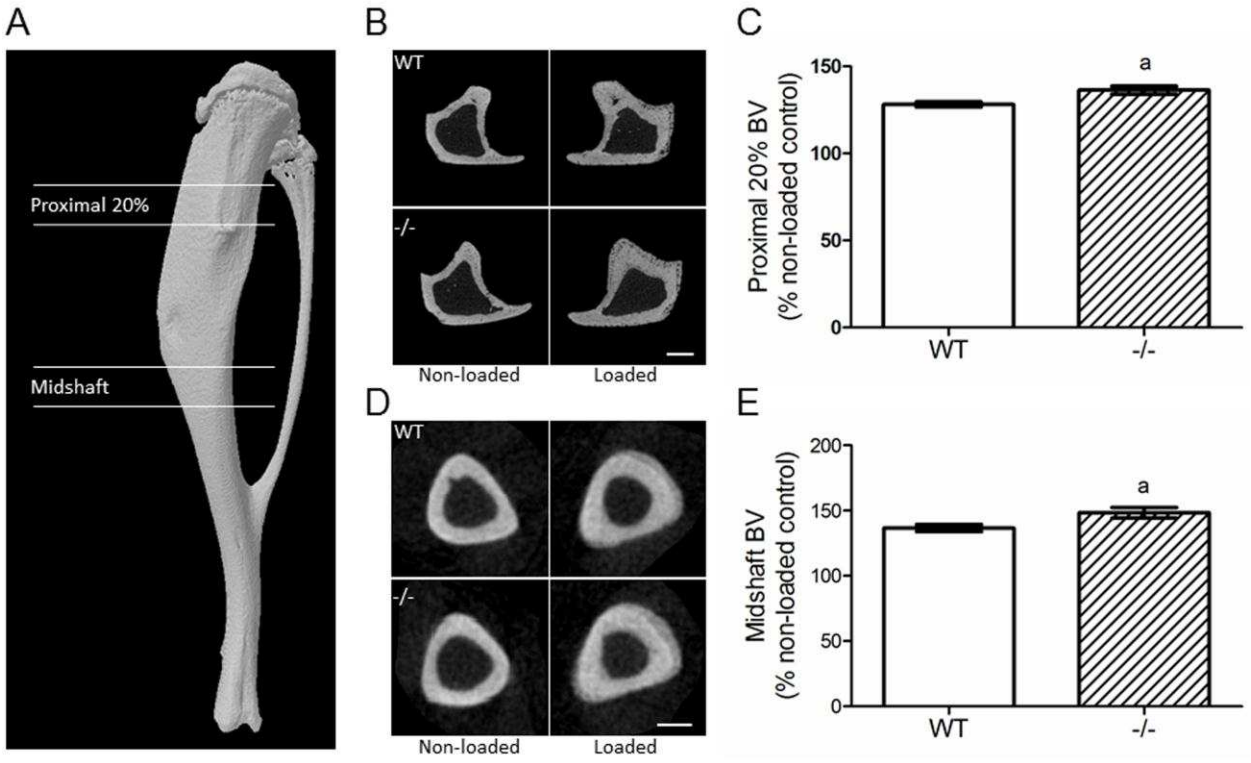
A
Proximal 20%
Midshaft
B
WT
-/-
Non-loaded
Loaded
C
Proximal 20% BV
(% non-loaded control)
150
100
50
0
a
WT
-/-
D
WT
-/-
Non-loaded
Loaded
E
Midshaft BV
(% non-loaded control)
200
150
100
50
0
a
WT
-/-

Figure 4

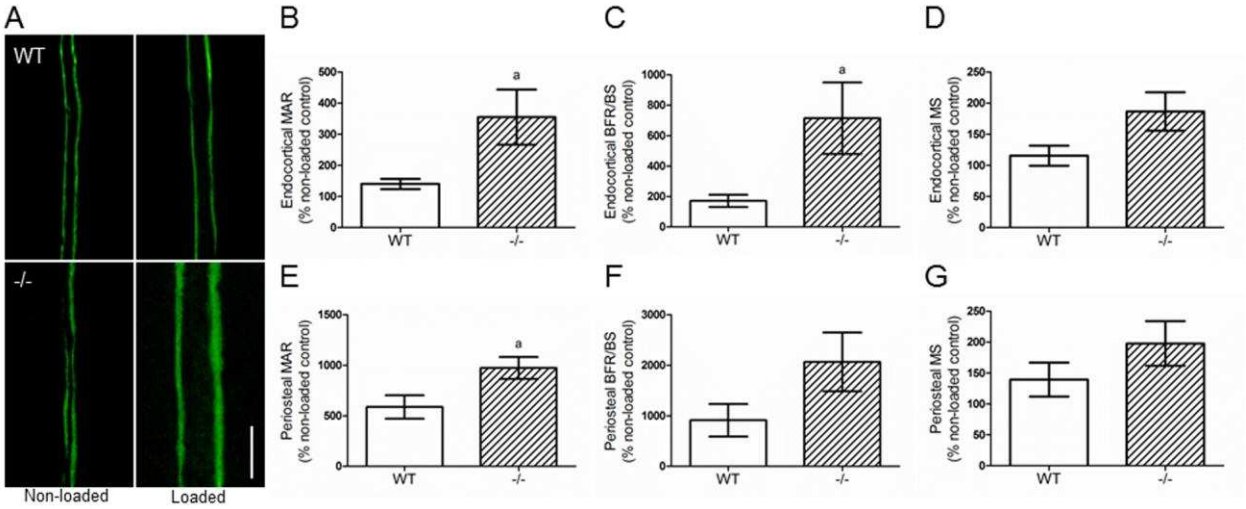
A
WT
-/-
Non-loaded
Loaded
B
Endocortical MAR (% non-loaded control)
a
WT
-/-
C
Endocortical BFR/BS (% non-loaded control)
a
WT
-/-
D
Endocortical MS (% non-loaded control)
WT
-/-
E
Periosteal MAR (% non-loaded control)
a
WT
-/-
F
Periosteal BFR/BS (% non-loaded control)
WT
-/-
G
Periosteal MS (% non-loaded control)
WT
-/-

Figure 5

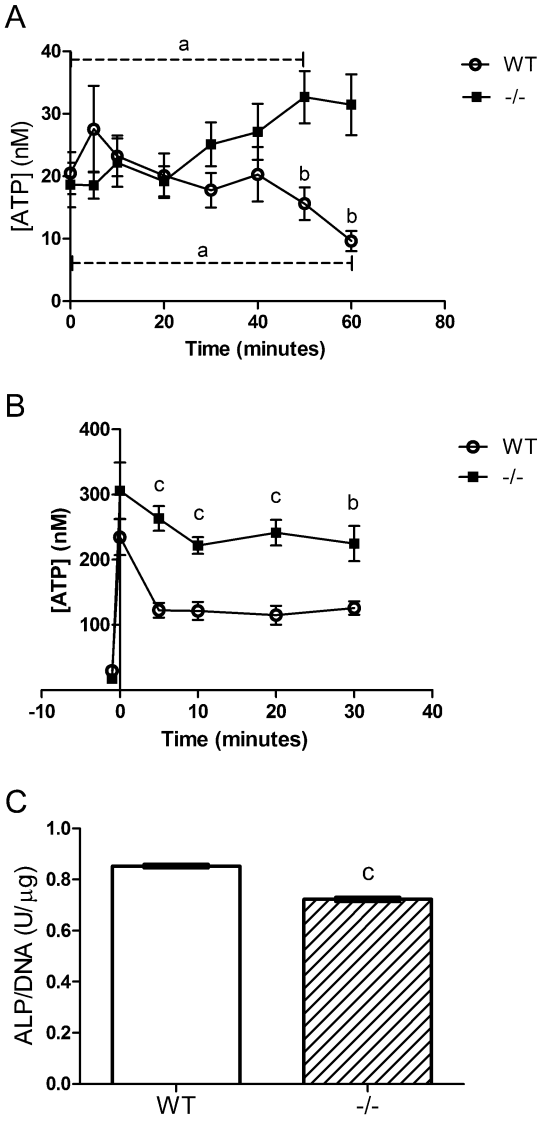
A
[ATP] (nM)
Time (minutes)
WT
-/-
a
a
b
b
B
[ATP] (nM)
Time (minutes)
WT
-/-
c
c
c
b
C
ALP/DNA (U/μg)
c
WT
-/-